Model Predictive Power Sharing Algorithm for Fuel Cell Integration in a Dual Inverter Electric Vehicle Drivetrain

Mehanathan Pathmanathan, Caniggia Viana, Sukhjit Singh, Peter W. Lehn
Department of Electrical and Computer Engineering
University of Toronto, Canada

Acknowledgement

This work was supported by the Natural Sciences and Engineering Research Council of Canada (NSERC) under Grant CRDPJ 513206-17.

Keywords

≪Fuel Cell≫, ≪Power Sharing≫, ≪electric vehicle≫, ≪drivetrain≫, ≪modeling≫.

Abstract

Fuel Cell hybrid electric vehicles require power electronic converter topologies and control algorithms which allow the slow dynamics and unidirectional nature of fuel cells to be respected throughout a drive cycle. This paper introduces a model predictive control algorithm which allows a dual inverter topology to achieve the required constraints for fuel cell integration in electric vehicles.

Introduction

The global push towards decarbonization can be facilitated by transportation electrification. Fuel cell hybrid electric vehicles (FCVs) which use a proton exchange membrane (PEM) hydrogen fuel cell stack as the primary EV energy source are one avenue to transportation electrification [1].

To avoid fuel cell damage due to the fuel starvation phenomenon, the rate of change of fuel cell power needs to be limited. Furthermore, fuel cells are unidirectional sources, meaning that they cannot absorb energy. These constraints make it impossible for a fuel cell to be the sole energy source of an EV, since an EVs drivetrain must be capable of achieving fast power dynamics to accelerate quickly, and must be able to absorb power during regenerative braking transients [2].

Accordingly, a secondary energy source is always present on FCVs. Commercial vehicles such as the Toyota Mirai use a battery pack to provide the instantaneous power needed for fast vehicle dynamics, and to absorb the power generated during regenerative braking transients [3]. Traditionally, a unidirectional DC/DC converter is used to connect the FC stack to the battery pack [4]. This DC/DC converter has a dual role of stepping up the fuel cell voltage, and coordinating the power flow of the fuel cell to ensure that the fuel cell power follows a slowly changing reference.

The presence of a dedicated DC/DC converter for FC integration adds weight and volume to the FCV, especially due to the magnetic energy storage stage which is needed. A method of achieving FC integration without the need of a dedicated DC/DC converter (and associated magnetics) is to use a dual inverter drivetrain (Fig 1a) [5, 6]. In this topology, an open-winding traction motor is used, with a three-phase, two-level inverter on each side of the motor. The FC is used as the DC energy source on one inverter, while the battery pack is used as the DC energy source of the other inverter. The ability to use lower-voltage traction modules with lower switching energy also provides the opportunity to reduce power electronic losses in the system [7].

An algorithm for control and modulation of the dual inverter is needed to ensure that the unidirectional, slowly changing reference of the fuel cell can be achieved. This paper introduces an approach utilizing

finite control set (FCS) model predictive control to achieve these goals as an alternative to the vector-based power sharing introduced in [6]. It is forseen that the ability of MPC to combine the dual objectives of motor torque production and FC power reference tracking into a single cost function could reduce the complexity of the control implementation relative to the approach of [6].

System Architecture

The fuel cell studied in the simulation section of this work is the Ballard FCmove [8]. The VI curve of this fuel cell is plotted using an exponential approximation in Fig. 1b, along with a linear approximation. The linear approximation allows the fuel cell to be modelled as an internal voltage source of 520 V and a series resistance of 0.85 Ω (E_{FC} and R_{FC} in Fig. 1a.)

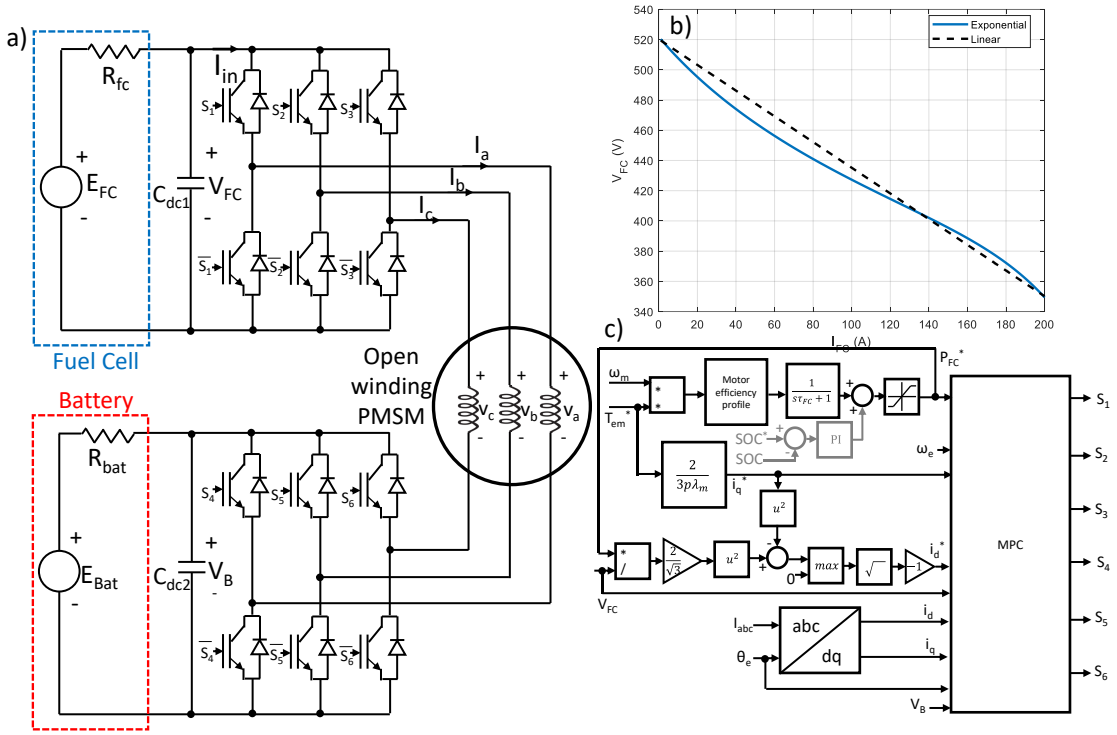

Fig. 1: Topology of proposed system (a), and Exponential model of Ballard FCMove V-I curve and linear model using E_{FC} and R_{FC} (b), and control diagram of the MPC based FC/battery dual inverter system (c)

Control Algorithm

The control diagram used in this study is shown in Fig. 1c. The predictive controller acts by selecting optimal switching states of the dual inverter in order to achieve regulation of the motor torque (via tracking reference dq currents) and fuel cell power. The following sections will describe the operation of the control algorithm.

Reference Generation

The fuel cell power reference (P^*_{FC}) is generated from low-pass filtering the motor mechanical power, as shown in Fig. 1c [2]. A battery SOC controller (shown in grey) can be used to increase or decrease the power reference. This controller is not implemented in this work, but is included in Fig. 1c for explanatory purposes. The saturation block in Fig. 1c) is used to limit the fuel cell power reference between its maximum and minimum values. A minimum power reference greater than zero is required to ensure that the fuel cell is not shut down while the FCV is idling, or the vehicle is performing regenerative braking. In the simulation section of this work, a minimum P^*_{FC} of 5 kW is used and a maximum P^*_{FC} of 50 kW are used.

The motor q-axis current reference is given by (using non-salient PMSM assumption):

$$i_q^* = \frac{2T_{em}^*}{3p\lambda_m} \tag{1}$$

p is the motor pole pairs, and T_{em}^* is the torque reference. For a non-salient PMSM not operating in the field weakening region, the d-axis current reference should normally be set to zero. In this paper, an exception to this rule exists during control events where a sharp reduction in torque reference magnitude is requested. From (1), it is apparent that i_q^* scales linearly with T_{em}^*. However, since P_{FC}^* is a low-pass filtered value of the drive mechanical power, it is apparent that P_{FC}^* can be larger than the mechanical power when a reduction in torque is requested.

The maximum power which can be extracted by from the fuel cell at a given torque reference is:

$$P_{FCM} = \frac{3}{2}|\vec{V_{FCM}}||\vec{I}| \tag{2}$$

$|\vec{V_{FCM}}|$ is the maximum possible value of the FC inverter voltage vector (considered to be $\frac{V_{FC}}{\sqrt{3}}$ in this work), while $|\vec{I}|$ is the magnitude of the motor current vector. The minimum current vector magnitude needed to ensure a fuel cell power reference can be delivered is:

$$I_{PS} = \frac{2P_{FC}^*}{\sqrt{3}V_{FC}} \tag{3}$$

In the above equation, V_{FC} is the FC terminal voltage. If the calculated i_q^* value from (1) is smaller than I_{PS}, a non-zero i_d^* is needed to ensure that the requested fuel cell power can be delivered. This i_d^* lengthens the current vector, increasing $|\vec{I}|$ so that it is equal to I_{PS} The required value of i_d^* is given by:

$$i_d^* = \begin{cases} 0 & |i_q^*| > |I_{PS}| \\ -\sqrt{(I_{PS})^2 - (i_q^*)^2)} & |i_q^*| < |I_{PS}| \end{cases} \tag{4}$$

The second row of (4) only uses the negative solution of i_d^* so the injected reactive current acts as a field weakening current for the motor.

Switching Vector Selection

A dual inverter has 64 (2^6) possible switching vectors. In order to minimize the computation time required by the predictive control algorithm, it is beneficial to reduce the number of switching states. The switching states shown in the Appendix (Table II) are used, which eliminate all redundancies and also non-redundant states which are not essential for operation of the predictive control algorithm. In this table the terms $S_{aFC}, S_{bFC}, S_{cFC}$ are the gating signals of the upper switches in the FC inverter and S_{aB}, S_{bB}, S_{cB} are the corresponding signals of the battery inverter.

Fig. 2a illustrates the voltage vectors in the $\alpha\beta$ frame for the motor voltage ($V_{\alpha\beta}$), as well as the FC and battery inverter voltage vectors individually ($V_{\alpha\beta FC}$) and $V_{\alpha\beta B}$) when the full set of 64 switching vectors is used where $V_B = 1pu$ and $V_{FC} = 0.7pu$. In contrast, Fig 2b shows the corresponding vectors achieved when the reduced set of vectors described in the Appendix are utilized. In the experimental implementation, operation with this reduced set of 30 switching vectors was found to result in a computation time of 46.8 μs, compared to 90.6 μs with the full set of 64 switching vectors, when a 200 MHz Texas Instruments F28379D digital signal processor was used as the control platform.

Motor Current Prediction

The motor current prediction algorithm evaluates the dq current values which will be generated by each of the switching states shown in the Appendix. As a starting point, a rotational transformation is applied to the motor $\alpha\beta$ components from each of the available switching vectors to obtain the dq voltages, using

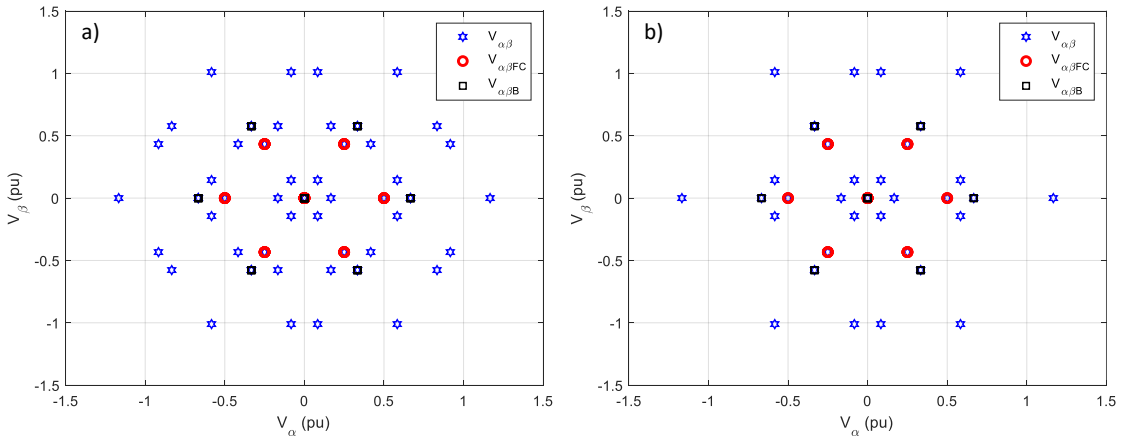

Fig. 2: Full set of available voltage vectors (a), reduced set utilized in this study (b) for a case where $V_{FC} = 0.75pu$, $V_B = 1pu$

the measured rotor electrical position θ_e:

$$\begin{bmatrix} v_d^{k+1} \\ v_q^{k+1} \end{bmatrix} = \begin{bmatrix} \cos\theta & \sin(\theta_e) \\ -\sin\theta & \cos(\theta_e) \end{bmatrix} \begin{bmatrix} v_\alpha^{k+1} \\ v_\beta^{k+1} \end{bmatrix} \tag{5}$$

The predicted motor d and q currents can be obtained by performing a forward Euler discretization on the differential equations describing the two-axis model of the PMSM:

$$i_d^{k+2} = (1 - \frac{R_s T_s}{L_d}) i_d^{k+1} + \frac{T_s}{L_d} v_d^{k+1} + \frac{\omega_e L_q T_s}{L_d} i_q^{k+1} \tag{6}$$

$$i_q^{k+2} = (1 - \frac{R_s T_s}{L_q}) i_q^{k+1} + \frac{T_s}{L_q} v_q^{k+1} + \frac{\omega_e T_s}{L_q} (L_d i_d^{k+1} + \lambda_m) \tag{7}$$

Please note that $k+2$ prediction is used in this study, meaning that the predicted currents will be two steps ahead from the measured current. The predicted one-step ahead d and q axes currents (i_d^{k+1} and i_q^{k+1}) are calculated using the optimal voltage vectors from the previous time step and measured dq current values in place of i_d^{k+1} and i_q^{k+1}. [9].

Fuel cell power prediction

The FC inverter DC current (I_{in} in Fig. 1a) is a function of the motor phase currents and fuel cell inverter switching functions. Its one step ahead value is given by:

$$I_{in}^{k+1} = S_{aFC} i_a^{k+1} + S_{bFC} i_b^{k+1} + S_{cFC} i_c^{k+1} \tag{8}$$

As shown in Fig. 1a, the voltage across the DC link capacitor is equal to the fuel cell terminal voltage. Thus, the predicted fuel cell voltage can be obtained by using a forward Euler approximation to discretize the first-order differential equation describing the DC-link capacitor voltage:

$$V_{FC}^{k+2} = \frac{T_s}{C_{dc}} (I_{FC}^{k+1} - I_{in}^{k+1}) + V_{FC}^{k+1} \tag{9}$$

In this equation, I_{FC}^{k+1} is the one-step ahead fuel cell current, given by:

$$I_{FC}^{k+1} = \frac{E_{FC} - V_{FC}^{k+1}}{R_{FC}} \tag{10}$$

Additionally, the $k+2$ fuell cell current can be calculated using V_{FC}^{k+2} in (10). Finally the two-step-ahead predicted FC power is obtained by $P_{FC}^{k+2} = I_{FC}^{k+2} V_{FC}^{k+2}$.

Cost function

The objective of the MPC algorithm is to select the switching state which minimized the error between control parameters (motor dq currents, P_{FC}) and their reference values. These errors can be expressed in terms of a cost function (where the current variables are in Amperes, and the power variables are in Watts):

$$g = (i_d^* - i_d^{k+2})^2 + (i_q^* - i_q^{k+2})^2 + k(P_{FC}^* - P_{FC}^{k+2})^2 \tag{11}$$

The variable k is the weighting function applied to the fuel cell power error (0.02 in this work). The optimal switching state is ultimately the switching state with the minimum value of g.

Simulation Results

A simulation model in PLECS blockset and Simulink was constructed to verify the performance of the proposed algorithm. The parameters of the proposed system are shown in Table I. A torque reference of 180 Nm was originally specified for the PMSM. This torque was achieved by requesting a i_q value of 190 A, with i_d = 0 A as can be seen from Fig. 2a. This torque causes the PMSM to accelerate from t = 0 s to t = 2.5 s, since the magnitude of the motor electromagnetic torque (T_{em}) is greater than that of the load torque (T_L, set to -100 Nm). At t = 2.5s, the torque reference is changed to 20 Nm, which causes i_q^* to become 25 A. At the same time, the load torque profile (T_L) is changed to be -20 Nm, which causes the motor speed to be constant. This reduction of T_{em} is achieved by a step reduction in i_q, as seen in Fig. 3. A negative i_d^* is injected at the time of the i_q^* reduction, to ensure the minimum current vector magnitude $|I_{PS}|$ (3) for attaining the FC power reference is maintained.

At t = 4 s, the motor torque reference is changed from 20 Nm to -180 Nm. At this time, the motor begins to brake, meaning that it is generating power. The fuel cell power drops to its minimum value of 5 kW, and maintains this value despite the power which is generated by the braking action of the motor. At this time, the battery power (P_{bat}) has a step decrease towards a minimum value of -40 kW, as the braking power of the generator and the FC power are absorbed by the battery.

Table I: Simulation parameters

Parameter	Description	Value
E_{FC}	Fuel cell internal voltage	520 V
R_{FC}	Fuel cell ESR from linear approx.	0.85 Ω
E_{Bat}	Battery internal voltage	400 V
C_{dc1}, C_{dc2}	DC link capacitance	4.5 mF
R_{bat}	Battery ESR	0.1 Ω
τ_{FC}	FC controller time constant	1 s
T_s	Sampling time	50 μs
$L_d = L_q$	Motor d and q inductances	800 μH
R_s	Motor phase resistance	45 mΩ
λ_m	Motor flux linkage	0.127 Wb

Experimental Results

A reduced scale experimental setup was built to verify the performance of the MPC algorithm (Fig. 3). The open-wound PMSM was fed by a dual inverter controlled by a Texas Instruments F28379D DSP. The two energy sources on the DC-links of the dual inverter were implemented using EA PSB750 power supplies. The R_{FC} and E_{FC} FC model elements depicted in Fig. 1a were implemented via the EA PSB750 internal resistance operating mode. In the experimental setup, E_{FC} was set to 150 V, R_{FC} was

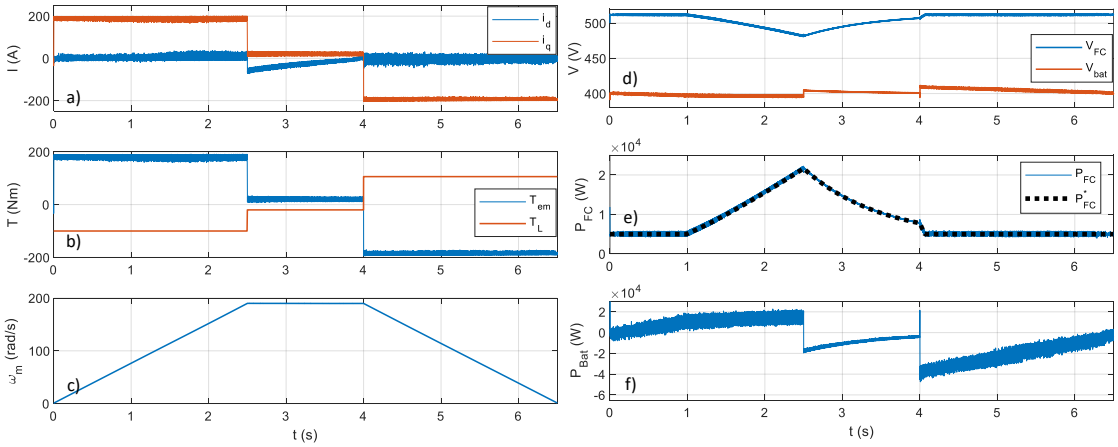

Fig. 3: Motor dq currents (a), torque (b), speed (c), FC and battery voltages (d), FC power reference and power (e), and battery power (f)

set to 1.667 Ω. The battery was modelled as a constant voltage 150 V source. Additionally, the prototype dual inverter was constructed with busbars designed to accommodate 500 μF DC-link capacitors. As such, the experiments were conducted with this value of capacitance.

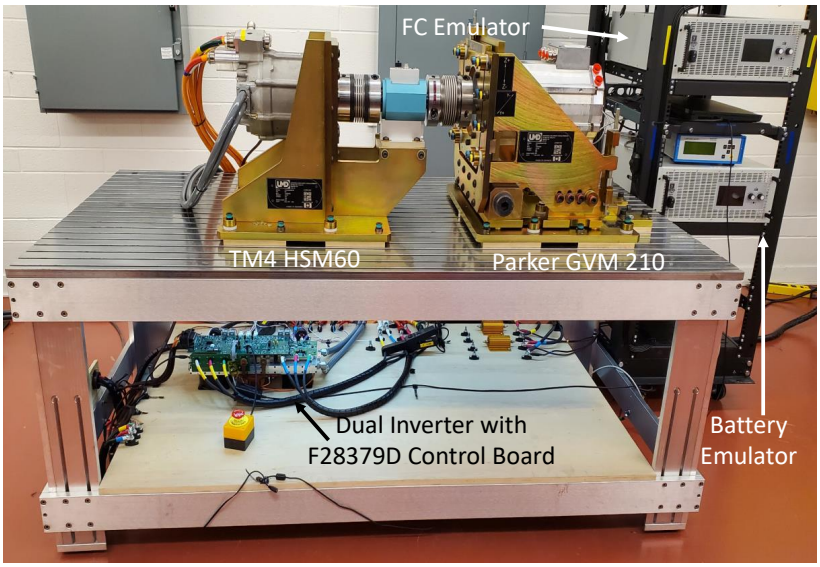

Fig. 4: Experimental setup used to verify predictive control algorithm

In Fig. 5a, results are shown for a regenerative transient in motor torque at a constant speed of 500 rpm. Prior to the transient, the motor was operating with a reference torque of 30 Nm. At the transient time, the reference was changed to -15 Nm. From CH4 in this figure, it is apparent that the torque changes rapidly at this time. CH1 and CH2 show the FC voltage and current respectively. A slow transition in FC voltage and current is noted, due to the influence of the low pass filter with time constant τ_{FC} which is used to generate the fuel cell power reference.

The motor phase 'A' current is provided as CH3. The magnitude of this current waveform does not drop rapidly when the regenerative transient is enacted. This is due to the injection of reactive current, which allows the fuel cell power to slowly ramp down even when mechanical power is reduced drastically, as described in by (4).

A second set of experimental results are shown in Fig. 5b, where the motor torque reference is changed from 10 Nm to 30 Nm at a speed of 500 rpm. In this case, the FC current and voltage once again

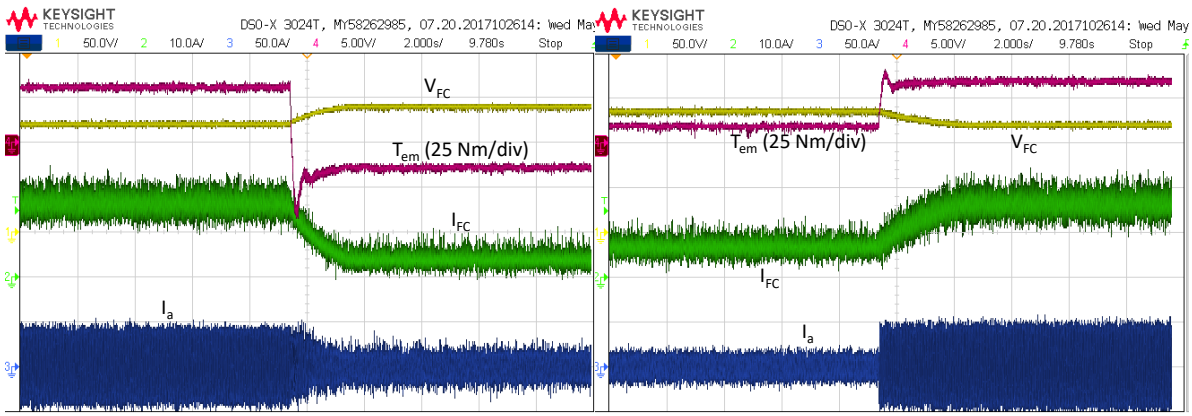

Fig. 5: Experimental results for +30 Nm to -15 Nm regenerative braking transient (a) and 10 Nm to 30 Nm torque increase transient at 500 rpm

change slowly due to the influence of the slowly-changing fuel cell power reference. In contrast with the previous experimental result, the magnitude of the phase 'A' current increases rapidly at the time of the torque transient. This is because no reactive current injection is needed to ensure that the fuel cell power can track its reference, during increases in current magnitude.

Conclusion

A finite control set model predictive control algorithm for a dual inverter drivetrain in a FCV is introduced. This algorithm allows fuel cell power reference tracking and motor torque reference tracking to be achieved simultaneously. In particular, this approach ensures that the fuel cell power tracks a slowly changing reference value, even when rapid torque (and hence power) dynamics are requested from the traction motor. Additionally, the algorithm ensures that the fuel cell power remains positive even when the motor performs regenerative braking.

Simulation results are presented showcasing the ability of the proposed algorithm in meeting these twin goals of fuel cell power tracking and motor torque control. Finally, experimental results are shown validating the practical performance of the proposed algorithm.

References

[1] U.R Prasanna, P. Xuewei, A.K Rathore, and K. Rajashekara, "Propulsion system architecture and power conditioning topologies for fuel cell vehicles," *IEEE Trans. on Ind. Elec.*, vol. 51, no. 1, pp. 640-650.

[2] J. Bauman, and M. Kazerani, "A comparative study of fuel-cell-battery, fuel-cell-ultracapacitor, and fuel-cell-battery-ultracapacitor vehicles," *IEEE Trans. on Vehicular Technology*, vol. 57, no. 2, pp. 760-769.

[3] Y. Hasuka, H. Sekine, K. Katano, and Y. Nonobe, "Development of boost converter for mirai," *SAE Techinical Paper*, pp. 1–6, 2015.

[4] N. Elsayad, H. Moradisizkoohi, and O. A. Mohammed, "A new single-switch structure of a dc-dc converter with wide conversion ratio for fuel cell vehicles: analysis and development," *IEEE Journal of Emerging and Selected Topics in Power Electronics*, vol. 8, no. 3, pp. 2785–2800, 2020.

[5] R. Shi, S. Semsar, and P.W. Lehn, "Single-stage hybrid energy storage integration in electric vehicles using vector controlled power sharing," *IEEE Trans. on Ind. Elec.*, vol. 68, no. 11, pp. 10623–10633, 2021.

[6] M. Pathmanathan, S. Semsar, C. Viana and P.W. Lehn, "Power Sharing Control Algorithm for Direct Integration of Fuel Cells in a Dual-Inverter Electric Vehicle Drivetrain," in *IEEE Transactions on Transportation Electrification*, vol. 8, no. 2, pp. 2490-2500, June 2022

[7] Y. Wang, M. Pathmanathan and P.W. Lehn, "Loss Comparison of Electric Vehicle Fuel Cell Integration Methods," International Symposium on Industrial Electronics (ISIE) 2022

[8] Ballard, "FCmoveHD Product Data Sheet,"[Online]. Available: https://www.ballard.com /docs/default-source/motive-modules-documents/fcmovetm.pdf?sfvrsn=6a83c3806

[9] J. Rodriguez, and P. Cortes, "Predictive Control of Power Converters and Electrical Drives," John Wiley and Sons, 2012.

[10] K.A. Corzine, S.D. Sudhoff, and C.A. Whitcomb, "Performance characteristics of a cascaded two-level converter," *IEEE Trans. on Energy Conv.*, vol. 14, no. 3, pp. 433–439, 1999.

Appendix

The dual inverter switching states which are utilized by MPC algorithm are shown in Table II below. S_{aFC}, S_{bFC} and S_{cFC} are the gating signals of the upper IGBTs in legs a, b and c of the FC inverter. Likewise, S_{aB}, S_{bB} and S_{cB} are the corresponding gating signals of the battery inverter. $v_{\alpha FC}$ and $v_{\beta FC}$ are the stationary reference frame voltages produced by the FC inverter (in terms of the FC voltage, V_{FC}). The stationary reference frame representation of the motor voltages (represented in terms of V_{FC} and the battery voltage, V_B are provided as v_α and v_β.

Table II: Switching states utilized in the fuel cell/battery dual inverter predictive controller

State No.	S_{aFC}	S_{bFC}	S_{cFC}	S_{aB}	S_{bB}	S_{cB}	$v_{\alpha FC}$	$v_{\beta FC}$	v_α	v_β
0	0	0	0	0	0	0	0	0	0	0
1	1	0	0	0	0	0	$\frac{2V_{FC}}{3}$	0	$\frac{2V_{FC}}{3}$	0
2	0	1	0	0	0	0	$-\frac{V_{FC}}{3}$	$\frac{V_{FC}}{\sqrt{3}}$	$-\frac{V_{FC}}{3}$	$\frac{V_{FC}}{\sqrt{3}}$
3	1	1	0	0	0	0	$\frac{V_{FC}}{3}$	$\frac{V_{FC}}{\sqrt{3}}$	$\frac{V_{FC}}{3}$	$\frac{V_{FC}}{\sqrt{3}}$
4	0	0	1	0	0	0	$-\frac{V_{FC}}{3}$	$-\frac{V_{FC}}{\sqrt{3}}$	$-\frac{V_{FC}}{3}$	$-\frac{V_{FC}}{\sqrt{3}}$
5	1	0	1	0	0	0	$\frac{V_{FC}}{3}$	$-\frac{V_{FC}}{\sqrt{3}}$	$\frac{V_{FC}}{3}$	$-\frac{V_{FC}}{\sqrt{3}}$
6	0	1	1	0	0	0	$-\frac{2V_{FC}}{3}$	0	$-\frac{2V_{FC}}{3}$	0
8	0	0	0	1	0	0	0	0	$-\frac{2V_B}{3}$	0
9	1	0	0	1	0	0	$\frac{2V_{FC}}{3}$	0	$\frac{2V_{FC}-2V_B}{3}$	0
14	0	1	1	1	0	0	$-\frac{2V_{FC}}{3}$	0	$\frac{-2V_{FC}-2V_B}{3}$	0
18	0	1	1	1	0	0	$-\frac{V_{FC}}{3}$	$\frac{V_{FC}}{\sqrt{3}}$	$\frac{V_B-V_{FC}}{3}$	$\frac{V_B-V_{FC}}{\sqrt{3}}$
19	1	1	0	0	1	0	$\frac{V_{FC}}{3}$	$\frac{V_{FC}}{\sqrt{3}}$	$\frac{V_{FC}+V_B}{3}$	$\frac{V_{FC}-V_B}{\sqrt{3}}$
20	0	0	1	1	0	0	$-\frac{V_{FC}}{3}$	$-\frac{V_{FC}}{\sqrt{3}}$	$\frac{V_B-V_{FC}}{3}$	$\frac{-V_{FC}-V_B}{\sqrt{3}}$
21	1	0	1	0	1	0	$\frac{V_{FC}}{3}$	$-\frac{V_{FC}}{\sqrt{3}}$	$\frac{V_{FC}+V_B}{3}$	$\frac{-V_{FC}-V_B}{\sqrt{3}}$
23	1	1	1	0	1	0	0	0	$\frac{V_B}{3}$	$-\frac{V_B}{\sqrt{3}}$
26	0	1	0	1	1	0	$-\frac{V_{FC}}{3}$	$\frac{V_{FC}}{\sqrt{3}}$	$\frac{-V_{FC}-V_B}{3}$	$\frac{V_{FC}-V_B}{\sqrt{3}}$
27	1	1	0	1	1	0	$\frac{V_{FC}}{3}$	$\frac{V_{FC}}{\sqrt{3}}$	$\frac{V_{FC}-V_B}{3}$	$\frac{V_{FC}-V_B}{\sqrt{3}}$
28	0	0	1	1	1	0	$-\frac{V_{FC}}{3}$	$-\frac{V_{FC}}{\sqrt{3}}$	$\frac{-V_{FC}-V_B}{3}$	$\frac{-V_{FC}-V_B}{\sqrt{3}}$
29	1	0	1	1	1	0	$\frac{V_{FC}}{3}$	$-\frac{V_{FC}}{\sqrt{3}}$	$\frac{V_{FC}-V_B}{3}$	$\frac{-V_{FC}-V_B}{\sqrt{3}}$
31	1	1	1	1	1	0	0	0	$\frac{-V_{FC}}{3}$	$\frac{-V_B}{\sqrt{3}}$
34	0	1	0	0	0	1	$\frac{-V_{FC}}{3}$	$\frac{V_{FC}}{\sqrt{3}}$	$\frac{V_B-V_{FC}}{3}$	$\frac{V_{FC}+V_B}{\sqrt{3}}$
35	1	1	0	0	0	1	$\frac{V_{FC}}{3}$	$\frac{V_{FC}}{\sqrt{3}}$	$\frac{V_B+V_{FC}}{3}$	$\frac{V_{FC}+V_B}{\sqrt{3}}$
36	0	0	1	0	0	1	$-\frac{V_{FC}}{3}$	$-\frac{V_{FC}}{\sqrt{3}}$	$\frac{V_B-V_{FC}}{3}$	$\frac{V_B-V_{FC}}{\sqrt{3}}$
37	1	0	1	0	0	1	$\frac{V_{FC}}{3}$	$-\frac{V_{FC}}{\sqrt{3}}$	$\frac{V_B+V_{FC}}{3}$	$\frac{V_B-V_{FC}}{\sqrt{3}}$
39	1	1	1	0	0	1	0	0	$\frac{V_B}{3}$	$\frac{V_B}{\sqrt{3}}$
40	0	0	0	1	0	1	0	0	$-\frac{V_B}{3}$	$\frac{V_B}{\sqrt{3}}$
42	0	1	0	1	0	1	$-\frac{V_{FC}}{3}$	$\frac{V_{FC}}{\sqrt{3}}$	$\frac{-V_B-V_{FC}}{3}$	$\frac{V_B+V_{FC}}{\sqrt{3}}$
43	1	1	0	1	0	1	$\frac{V_{FC}}{3}$	$\frac{V_{FC}}{\sqrt{3}}$	$\frac{V_{FC}-V_B}{3}$	$\frac{V_B+V_{FC}}{\sqrt{3}}$
44	0	0	1	1	0	1	$-\frac{V_{FC}}{3}$	$-\frac{V_{FC}}{\sqrt{3}}$	$\frac{-V_B-V_{FC}}{3}$	$\frac{V_B-V_{FC}}{\sqrt{3}}$
45	1	0	1	1	0	1	$\frac{V_{FC}}{3}$	$-\frac{V_{FC}}{\sqrt{3}}$	$\frac{V_B-V_{FC}}{3}$	$\frac{V_B-V_{FC}}{\sqrt{3}}$
47	1	1	1	1	0	1	0	0	$\frac{-V_B}{3}$	$\frac{V_B}{\sqrt{3}}$
48	0	0	0	0	1	1	0	0	$\frac{2V_B}{3}$	0
49	1	0	0	0	1	1	$\frac{2V_{FC}}{3}$	0	$\frac{2V_{FC}+2V_B}{3}$	0
54	0	1	1	0	1	1	$-\frac{2V_{FC}}{3}$	0	$\frac{2V_B-2V_{FC}}{3}$	0